molbank

MDPI

Communication

Crystal Structures of Half-Sandwich Ru(II) Complexes, [(η⁶-*p*-Cymene)(3-chloro-6-(1*H*-pyrazol-1-yl)pyridazine)Ru(X)]BF_4, (X = Cl, Br, I)

Allen Mambanda [1,*], Peter Ongoma [2], Joel Gichumbi [3], Reinner O. Omondi [1,4], Leigh A. Hunter [1] and Amos K. Kanyora [2,*]

jgichumbi@chuka.ac.ke

1 School of Chemistry and Physics, University of KwaZulu-Natal, Private Bag X01, Scottsville, Pietermaritzburg 3209, South Africa
2 Department of Chemistry, Egerton University, Egerton P.O Box 536-20115, Kenya
3 Department of Physical Sciences, Chuka University, Chuka P.O. Box 109-60400, Kenya
4 Department of Chemistry, University of Cape Town, Rondebosch 7701, South Africa
* Correspondence: mambanda@ukzn.ac.za (A.M.); kimem.aka12@gmail.com (A.K.K.)

Abstract: Herein, we report the synthesis and single-crystal X-ray structures of three (η⁶-*p*-cymene)Ru(II) tetrafluoroborate salts, viz., [(η⁶-*p*-cymene)(3-chloro-6-(1*H*-pyrazol-1-yl)pyridazine)Ru(X)]BF_4, (X = Cl, Br, I), **Ru1-3**. They were prepared by the reactions of [(η⁶-*p*-cymene)Ru(μ-X)(X)]$_2$, (X = Cl, Br, I) with two-mole equivalents of 3-chloro-6-(1H-pyrazol-1-yl)pyridazine, under inert conditions at ambient temperatures, and subsequently precipitated by the addition of excess BF_4^- ions. Orange crystalline precipitates were obtained in good yields, from which the respective single crystals for X-ray diffraction analysis were recrystallized by slow evaporation from their methanolic/diethyl ether solutions. The Ru(II) complexes were characterized by various spectroscopic techniques and chemical methods, which included FTIR, $^1H/^{13}C$ NMR, UV-visible absorption, mass spectrometry, and elemental analysis. The molecular structures were solved by single-crystal X-ray crystal diffraction analysis. The complexes crystallized in the monoclinic crystal system in the $P2_1/c$ **(Ru1-2)** and $P2_1/n$ **(Ru3)** space groups. Density Functionals Theoretical (DFT) calculations were performed in methanol to gain an understanding of the electronic and structural properties of the complexes. Trends in the data metrics were established, and selected data were compared with the diffraction data. The electrophilicity indices of **Ru1-3** follow the order **Ru3** > **Ru2** > **Ru1**, and the trend is in line with their anticipated order of reactivity towards nucleophiles.

Keywords: single-crystal X-ray structure; 3-chloro-6-(1H-pyrazol-1-yl)pyridazine; pyridazine; *p*-cymene ruthenium(II) complexes; DFT geometry optimized structure

Citation: Mambanda, A.; Ongoma, P.; Gichumbi, J.; Omondi, R.O.; Hunter, L.A.; Kanyora, A.K. Crystal Structures of Half-Sandwich Ru(II) Complexes, [(η⁶-*p*-Cymene)(3-chloro-6-(1*H*-pyrazol-1-yl)pyridazine)Ru(X)]BF_4, (X = Cl, Br, I). *Molbank* **2022**, *2022*, M1477. https://doi.org/10.3390/M1477

Academic Editor: Kristof Van Hecke

Received: 6 August 2022
Accepted: 24 October 2022
Published: 31 October 2022

Publisher's Note: MDPI stays neutral with regard to jurisdictional claims in published maps and institutional affiliations.

1. Introduction

Reactions of suitable precursor complexes of iridium (Ir), rhodium (Rh), ruthenium (Ru), or osmium (Os) with η⁶-arene ligands form chemically stable halogen-bridged intermediates, from which the monomeric half-sandwich- or piano stool-structured complexes, [(η⁶-arene)M (κ²-N,N′-*L*)X]Y (M = Ir(I), Rh(1), Ru(II), or Os(II); X = halide; Y = a counter anion, and N,N′-*L* = bidentate with N-donor atoms) are formed by the 1:2-mole ratio reaction between the respective intermediates with the N,N′-bidentate ligand [1]. These reactions proceed under mild conditions to form the half-sandwich complexes in good yields. The π-face coordinated η⁶-arene ligand brings extra chemical stability to the complexes. It π-donates its ring electrons to the metal center, forming three strong M-C bonds. It also confers necessary hydrophobicity to the coordination shell, stabilizes the oxidation state of the metal ion, as well as modulates the lability of the co-ligand. Consequently, the reactivity of the complex towards substitution of the labile co-ligand by nucleophiles also depends on the electronic properties of the coordinated η⁶-arene non-leaving ligand. Most

of these cationic complexes have sufficient aqueous solubility despite the hydrophobicity of the η^6-arene and ancillary ligand, *L*. These complexes, therefore, exhibit a suitable hydro-lipophilicity balance, which lends them suitable for many biomedical applications [2].

Current research efforts are aimed at developing Ru(III/II) complexes as alternatives to Pt(II) anticancer metallodrugs [3–11]. Ru(III) complexes such as NAMI-A, KP1019, and many other cytotoxic Ru(III) complexes [7,9,10] are thought to be anticancer prodrugs. Under the anoxic conditions of most cancer cells, they are reduced to their more reactive and active Ru(II) analogues [8]. Recently, promising cytotoxic Ru(II) complexes bearing an η^6-arene, an ancillary, and a chloro (as the labile ligand) have been developed. Lead cancer cytotoxic examples in this group include RAPTA-C [12,13] and RM175 [3]. The former bears a bulk 1,3,5-triaza-7-phosphaadamantane (PTA) as the ancillary ligand, while an N,N′ bidentate (ethylenediamine) ligand features in the latter. These exemplary η^6-arene Ru(II) complexes exhibit equivalent and in some cases better antitumor activities, reduced toxicity, low cross-resistance to cisplatin-resistant (Cis^{R}Pt) cell lines, and better aqueous solubility. The aforementioned chemical properties place η^6 arene Ru(II) complexes at the center stage for concerted research to attain more effective chemotherapeutic regimens.

The seminary work of Sadler et al. [14] on the effect of the leaving ligand on the cancer antiproliferation activity of the [(η^6-arene)(azo/aminopyridine-κ^2-N,N′)Ru/Os(II)X]$^+$, (X = Cl, I) complexes was a landmark testimony to the impact of the co-ligand on cytotoxicity. The complexes were designed to have the halide (Cl^-, I^-) as the activation site. Their rate of substitution by bio-nucleophiles (and hence the cytotoxic activity) would be modulated by the non-leaving ligands. The iodo analogues were found to be more cytotoxic compared to their chloro counterparts. The former analogues had better cellular accumulation profiles (in membranes and associated organelles) than the latter and were less cross-resistant to a Cis^{R}Pt cell line. The results demonstrated how a careful choice of the leaving group in the η^6-arene Ru(II) complexes can be useful for fine-tuning the pharmacological kinetics, cellular accumulation rates, and subsequent compartmentalization. These factors were attributed cooperatively to the enhanced chemotherapeutic effect for the iodo analogues.

In this work, three η^6-arene ruthenium(II) complexes of the form [(η^6-*p*-cymene)(3-chloro-6-(1*H*-pyrazol-1-yl)pyridazine)Ru(X)]BF_4, (X = Cl, Br, I), **Ru1-3**, were synthesized. Their molecular structures are shown in Figure 1. The aromaticity of the 6-(pyrazol-1-yl)pyridazine, (pzn-pdzn) is stabilized by electron-withdrawing groups such as the chloro on the 3-position of the pdzn ring in the coordinated bidentate of the synthesized complexes [15]. Unlike pyridine (pK_a = 5.3), which is known to be a strong base and strong acceptor of electron density from metal-centered *d*-orbitals, the donor/acceptor properties of pdzn as a ligand are not well understood. Pdzn is a popular pharmacophore sub-structure of several therapeutic drugs [16]. Examples include cefozopran, cadralazine, minaprine, pipofezine, and hydralazine. All these were the pull factors in choosing pdzn as a substructure on one of the non-leaving ligands of the studied Ru(II) complexes. The substitutional lability of the complexes was varied by changing their halide co-ligand to study the correlation between the reactivity of these complexes. We report and discuss the synthesis and single crystal X-structures of these complexes. Geometry-optimized data computed at the Density Functional Theory (DFT) level were compared with the crystal structure data and employed to give insight into the electronic and structural properties of complexes.

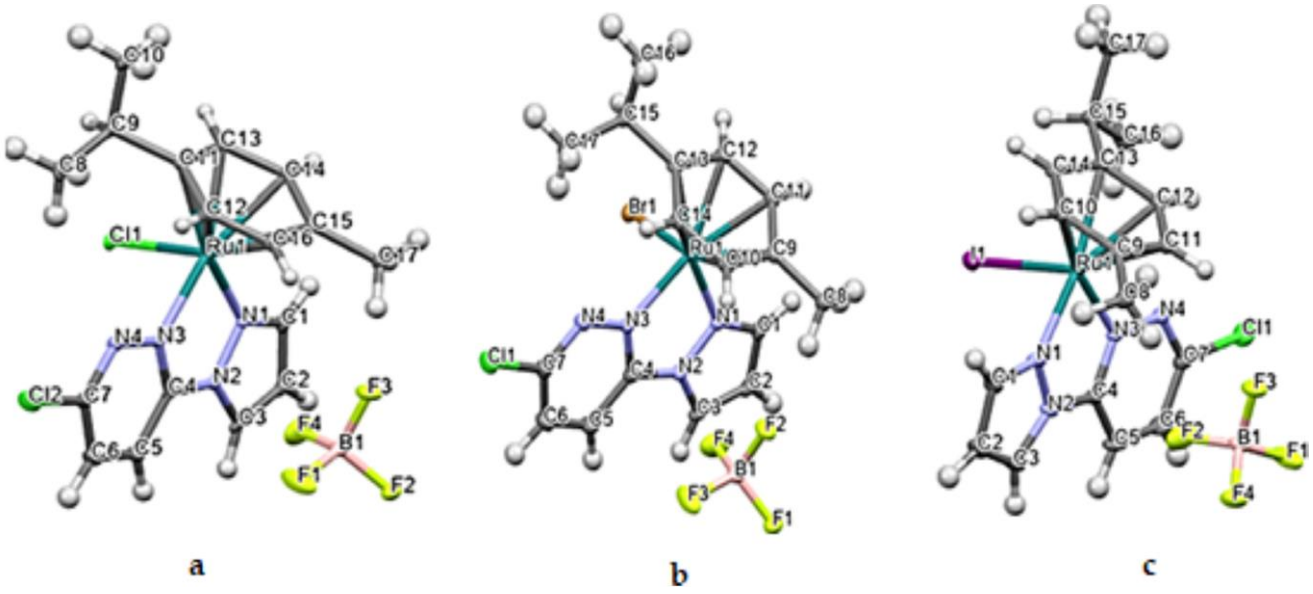

Figure 1. The Ortep diagrams of the Ru(II) complexes, [(η⁶-*p*-cymene)(3-chloro-6-(1H-pyrazol-1-yl)pyridazine)Ru(X)]BF_4, (**a**) **Ru1** (X = Cl); (**b**) **Ru2** (X = Br); (**c**) **Ru3** (X = I), showing their asymmetric units. The displacements of atoms are shown at the 50% probability level.

2. Results and Discussion

*2.1. Crystal Structures of **Ru1-3***

Suitable single crystals of **Ru1-3** for X-ray diffraction measurements were afforded by slow evaporations of concentrated methanol/diethyl ether (MeOH/Et_2O) solutions, and their molecular structures were solved by crystallographic analysis. The thermal ellipsoids (at 50% probability) depicting the molecular structures of the three complexes are shown in Figure 1. Data on the cell dimensions and other details on the data collection, refinement, and key structural parameters are presented in Table 1. Selected bond lengths and angles are presented in Table 2.

Complexes **Ru1-3** were crystallized from their respective MeOH/Et_2O solutions as non-solvated salts comprising the respective cation of the general formula [(η⁶-*p*-cymene)(3-chloro-6-(1*H*-pyrazol-1-yl)pyridazine)Ru(X)]$^+$ (X = Cl, Br, I), and BF_4^- as the counter anion. The structures are as depicted in 1. All three complexes assume a pseudo-octahedral geometry, which is widely reported for η⁶-arene Ru(II) half-sandwich-shaped complexes [11,12,14,17]. Characteristic of these complexes is the facial π-coordination of the η⁶-arene, leaving three (for octahedral) and in some cases two (for trigonal-/square pyramidal) coordination vacancies on the d^6 Ru(II) metal ion. The arene for these Ru(II) complexes is η⁶-cymene (η⁶-cym) and forms three nearly equivalent Ru-C π-bonds. The Ru to η⁶-cym $_{centroid}$ bond distances are 1.676 Å (**Ru1-2**) and 1.679 Å (**Ru3**), respectively, and are within the range reported for similar structured Ru(II) complexes [18]. These short centroid bond distances and the strong Ru-C π-bonds render them robust complexes with remarkable thermodynamic stability against hydrolysis or nucleophilic attack under ambient or aqueous conditions. These attributes make η⁶-arenes appealing ligands for stabilizing d^6 organometallic complexes for various applications, including in the biomedical field [11,12,14,16,17]. The remaining coordination vacancies are occupied by the halide as the labile co-ligand, and the 3-chloro-6-(1*H*-pyrazol-1-yl)pyridazine bidentate via its $N3_{pdzn}$, $N1_{pzn}$ donor atoms. The latter forms a five-membered chelate ring with the Ru(II) ion.

Table 1. Summary of the crystal metric data for **Ru1-3**.

Chemical Formula	$C_{17}H_{19}BCl_2F_4N_4Ru$	$C_{17}H_{19}BBrClF_4N_4Ru$	$C_{17}H_{19}BClF_4IN_4Ru$
M	538.14	582.60	629.59
T (K)	104	100	102.6
Crystal system	Monoclinic	Monoclinic	Monoclinic
Space group	$P2_1/c$	$P2_1/c$	$P2_1/n$
Unit cell dimensions			
a/Å	14.0177(5)	14.2238(3)	14.5324(3)
b/Å	10.6465(4)	10.6770(2)	10.7441(2)
c/Å	14.9362(5)	15.1270(3)	15.1862(3)
α/°	90	90	90
β/°	115.6560(10)	117.1390(10)	117.1050(10)
γ/°	90	90	90
Volume (Å^3)	2009.30(12)	2044.37(7)	2110.72(7)
Z	4	4	4
d_{cal} g/cm^3	1.779	1.893	1.981
Absorption coefficient (mm $^{-1}$)	9.206	10.136	19.085
F(000)	1072	1144	1216
Crystal size (mm^3)	0.656 × 0.395 × 0.295	0.285 × 0.130 × 0.125	0.240 × 0.130 × 0.125
2θ range for data collection (°)	6.996 to 142.948	6.984 to 135.992	6.98 to 136.082
Index ranges	$-16 \le h \le 16$, $-12 \le k \le 12$, $-18 \le l \le 17$	$-17 \le h \le 16$, $-11 \le k \le 10$, $-18 \le l \le 15$	$-17 \le h \le 17$, $-12 \le k \le 12$, $-18 \le l \le 18$
$N_{(hkl)}$, $N_{(hkl)unique}$, R_{int}	34776, 3815, 0.0419	25766, 3638, 0.0266	24963, 3808, 0.0318
Data/restraints/ Parameters	3815/0/265	3638/0/265	3808/0/265
Goodness-of-fit on F^2	1.17	1.132	1.11
Final R indices [$I \ge 2\sigma$ (I)]	R_1 = 0.0313, wR_2 = 0.0794	R_1 = 0.0188, wR_2 = 0.0469	R_1 = 0.0183, wR_2 = 0.0424
Final R indices [all data]	R_1 = 0.0313, wR_2 = 0.0794	R_1 = 0.0190, wR_2 = 0.0470	R_1 = 0.0186, wR_2 = 0.0425
Largest diff. peak/hole/e Å $^{-3}$	0.79/−1.58	0.55/−0.64	0.53/−0.72

Table 2. Selected bond length/Å and angles (°) from the crystal data for **Ru1-3**.

Complex	$C_{17}H_{19}BCl_2F_4N_4Ru$	$C_{17}H_{19}BBrClF_4N_4Ru$	$C_{17}H_{19}BClF_4IN_4Ru$
		Length (Å)	
Ru1-‡X1	2.3920(6)	2.5228(2)	2.6996(2)
Ru1-N1$_{pzn}$	2.080(2)	2.0718(17)	2.073(2)
Ru1-N3$_{pdzn}$	2.079(2)	2.0712(17)	2.0743(19)
Ru-Cym$_{centroid}$	1.676	1.676	1.679
		Angle (°)	
N1-Ru1-X1	84.03(7)	86.02(5)	82.85(6)
N3-Ru1-X1	84.61(7)	83.50(5)	88.44(6)
N3-Ru1-N1	76.18(9)	76.33(7)	76.19(8)

‡ X = Cl (**Ru1**); Br (**Ru2**); I (**Ru3**).

Coordination inorganic chemists are enchanted by the geometric distortions (conformational arrangement) of the octahedral η^6-arene-bearing complexes of Ru(II) such as **Ru1-3**. They liken the distortion of the geometry to a 'piano stool'. The facially coordinated η^6-cym is akin to the illusory 'seat' of the stool. The halide (X = Cl, Br, or I for **Ru1-3**), the N3$_{pdzn}$, N1$_{pzn}$ donor arms/atoms of the bidentate, are conformationally pronged onto the feet of the pseudo legs of the stool [5,6,14,17–21]. Despite this dramatic distortion from

the perfect octahedral geometry, these η⁶-arene complexes have sufficient chemical and thermal stability.

The pzn and the pdzn rings of the N,N′-bidentate ligand remain coplanar upon their chelation to the Ru(II) ion. The N_1-N_2-C_4-N_3 torsion angles are near zero and equal to −0.1(9)°, −0.8(3)°, and −5.4(3)° for **Ru1-3,** respectively. The Ru-N bond lengths of the compounds lie between 2.0712(17) and 2.080(2) Å, which are similar to those reported for other η⁶-arene Ru(II) complexes with N,N′ donor ligands [5,6,14,17–21]. The N-Ru-N bond angles range from 76.18(9)° to 76.33(9)°, while the N-Ru-X bond angles range from 83.50(5)° to 88.44(6)°. These ranges are similar to those reported for related η⁶-arene Ru(II) complexes with N,N′ bidentate ligands [20]. The Ru-X bond lengths increase as expected in the order Ru-Cl (2.3920(6) Å) [14,17–19], Ru–Br (2.5228(2) Å [11,22], and Ru–I (2.6996(2) Å) [11,14,23] for **Ru1-3** in line with the size of the labile ligand and the increase in the polarizability of the Ru-X bond. The bond lengths are comparable to those reported for related compounds: Ru–Cl [24], Ru–Br [22], and Ru–I [23]. The lengths and angles of all C—C, C—N, and B—F bonds are within the expected ranges for (N,N/O-bidentate)(η⁶-cym)Ru(II) complexes [3]. There are many inter/intramolecular interactions in the solid state of these Ru(II) borate salts (refer to Table S11 for a list of selected stabilizing short contacts or non-conventional hydrogen bonds). Some of these interactions occur between fluorine and hydrogen atoms of *p*-cym. Examples are the F . . . H–C short contact bonds (e.g., C17–H17···F3B, *d* = 2.868(4) for **Ru1**, while for **Ru2** and **Ru3**, similar non-conventional hydrogen bonds occur between the leaving group (X) and the hydrogen atom of the neighboring cation in the lattice, as exemplified by the C–H17 . . . Br1 = 3.024 Å and C16-H16 . . . I1 = 3.67 Å. A noteworthy difference in the relative conformational geometry and orientation of the ligands around the Ru(II) metal center is that the pzn and pdzn rings of **Ru3** are coordinated in contrastingly distinct orientations (when referenced to the orientations of substituents on the cymene) to that of the same rings in **Ru1-2**, as well as the analogue of **Ru1** reported in [18]. It is unclear what drives the difference in the orientations of the two non-leaving ligands which incidentally put these complexes in two coordinational or configurational sub-domains. In **Ru3**, the propyl group of the *p*-cym is oriented closer to the larger ring of the pdzn ligand, which seems to increase electron–electron repulsion between the groups, leading to a longer Ru-$C_{Cym(centroid)}$ distance for **Ru3** relative to that of either **Ru1** or **Ru2**. Contrastingly, the methanolic solutions afforded orange crystalline salts of **Ru1-3**. This is an indication that the coordinated halide ligand has little or no influence on the strength of the crystal field, and this is supported by the invariance in the magnitude of the HOMO-LUMO energy band gap (Table 3). The trend in the DFT-calculated data shows that there is no significant difference in the band gap energies of the three complexes. The commonality in the color of the salts of homologous halo-Ru(II) complexes was also reported for a series of [(η⁶-arene)Ru(II)]N-N′)X]⁺, X = Cl, Br and I complexes [11]. Only when the counter ion in the analogous salts of **Ru1** was changed from BF_4^- to PF_6^- was there a distinct color change from orange to yellow [18].

Table 3. DFT-calculated data for complexes **Ru1**-**3**.

Parameter	Ru1	Ru2	Ru3
HOMO-LUMO energy/eV			
−(LUMO), eV	3.164	3.162	3.150
−(HOMO), eV	6.513	6.417	6.254
Band gap, ΔE, eV	3.349	3.255	3.104
Global electrochemical parameter			
Chemical hardness (η)	1.675	1.627	1.552
Chemical potential (μ)	−4.838	−4.790	−4.702
Chemical softness (σ)	0.597	0.614	0.644
Electronegativity (χ)	4.838	4.790	4.702
Electrophilicity index (ω)	6.988	7.048	7.122

Table 3. *Cont.*

Parameter	Ru1	Ru2	Ru3
Nucleophilicity (ϵ)	0.143	0.142	0.140
Dipole moments (NBO) charge	7.8607	8.5126	9.1474
Ru	+0.090	−0.057	−0.130
X	−0.295	−0.213	−0.110
N1	−0.184	−0.186	−0.188
N3	−0.211	−0.213	−0.215

2.2. Spectroscopic Data

The molecular structures of the N,N′-bidentate ligand and its complexes Ru1-3 in solution were probed by $^{1}H/^{13}C$ NMR spectra and 2D-NMR techniques (correlation spectroscopy (COSY) and the heteronuclear single quantum coherence (HSQC)). NMR data are useful in elucidating the molecular structure behavior of compounds in solution. The $^{1}H/^{13}C$ NMR data for the ligand and the complexes are listed in the experimental section and their respective spectra are given in Figures S2–S7 (Supplementary Materials), respectively. The ^{1}H NMR resonances for the free ligand (Figure S1) appear upfield relative to those of **Ru1-3**. The $^{1}H/^{13}C$ NMR spectra of **Ru1-3** show common chemical shifts in the resonances of the ^{1}H and ^{13}C nuclei. This is an indication that the variation in the halide co-ligand has little or no influence on the electronic environment of the spins of the nuclei of the two coordinated non-leaving ligands. The 3J-constants of non-singlet peaks/(hyperfine-split resonances) in the ^{1}H NMR spectra of **Ru1-3** (Figures S2–S4) were used to confirm correlated protons in distinctive chemical environments of the complexes. The ^{1}H spectrum of **Ru3** features four common resonance (absorption) peaks while **Ru1** and **Ru2** have three peaks in the range of 5.90–6.30 ppm. The chemical equivalence of four protons due to the C_2-symmetry of the facially coordinated η^6-cym is broken by spin coupling with the diastereotopic protons of methyl groups of the isopropyl moiety. Additionally, the pseudo-octahedral (piano stool) arrangement of four different ligands around the Ru(II) ion makes the latter a chiral center. Thus, the complexes will exhibit stereoisomerism that breaks the C_2-symmetry of the cym and its spin resonance absorption [17]. The resonance peaks of the three protons of pzn and two of pdzn appear as five resonance peaks downfield (δ = 7.16–9.18 ppm), attributed to the ^{1}H nuclei on the C=N, C-N, C=C groups and those of the η^6-cym, respectively. As expected, these peaks were slightly deshielded compared to that of the free ligand (Figure S1), which ranges between 6.69 and 8.80. The aliphatic protons of the cym appear at 2.79 ppm (*m*, $_{1}H_{CH(CH3)2}$), 2.12 ppm (*s*, $3H_{methyl}$), and 1.15 ppm (*dd*, $2 \times 3_{Hmethyl\ isopropyl}$). The total number of carbon atoms and the range of their chemical shifts (ppm) agree with the different possible bonding environments of the C nuclei of the ligand framework for the proposed structures. Curiously, the aromatic resonances for the η^6-cym protons do not feature as two doublets as in the spectrum of the respective dimer precursors.

The 1D NMR data were corroborated by those of the COSY, HSQC, and other related correlated techniques, and these data are presented only for **Ru3** (refer to Figure S9 and Table S1). The absence of the $^{1}H/^{13}C$ cross peaks for C4, C7 (N,N-bidentate) and C8, C11 (cym) in the HSQC of **Ru3** (see Figure S9a, and for the carbon numbering, see Figure S8) confirms the quaternary nature of these carbons. The correlation assignments of the rest of the $^{1}H/^{13}C$ chemical shifts are consistent with the proposed structure of **Ru3** and its two analogues. These assignments were further corroborated by the COSY data (Figure S9b and Table S1). In the COSY map of **Ru3**, common $^{1}H/^{1}H$ cross-peaks are observed between the absorption resonances of protons on the C1/C2, C2/C3 (pzn), C5/C6 (pdzn), and C9/C10, C12/C13, C15/C16, C15/C17 (cym), showing that their carbons are bonded together (Figure S9a). Data of the correlated protons and their mutual coupling constant (^{3}J) are given in Table S1.

The chemical purity of **Ru1-3** was checked by elemental (CHNS) analysis while their structural elucidation in the solution was accomplished by various spectroscopic techniques. The elemental compositions of **Ru1-3** were within 5% of their theoretically calculated data (see the elemental data listed in the experimental section). This confirmed the high purity of the crystalline salts of **Ru1-3**.

Direct electro-spraying of solutions **Ru1-3** (in methanol/0.1% formic/formate buffer) yielded ion peaks at *m/z* values of 451 amu (100%), 497 amu (100%), and 543 amu (100%) in their low-resolution mass spectra (Figures S10–S12). The zoomed-out peaks (see insets in Figures S10–S12) exhibit isotopic distribution patterns that are comparable to the theoretical patterns for the respectively calculated formulas. The matched isotopic pattern for each serves as a structural fingerprint for confirming the identity (as observed in the nominal masses of the respective pseudo molecular ions of **Ru1-3** when the isotopic distribution of the elements for each complex is considered). These observed mass spectral data (Figures S10–S12) are attributed to their respective pseudo-protonated molecular ions: $[C_{17}H_{19}ClN_4RuCl + H]^+$ (for **Ru1**), $[C_{17}H_{19}ClN_4RuBr + H]^+$ (for **Ru2**), and $[C_{17}H_{19}ClN_4RuI + H]^+$ (for **Ru3**).

UV–visible electronic absorption spectra of the complexes **Ru1-3** in solution are depicted in Figure S13. All the electronic spectra of the complexes show similar spectral bands to those reported for other pseudo-octahedral complexes [25]. Characteristic absorption peaks include the medium-intensity bands in the region 250–260 nm, which are assigned to π–π* electronic transitions. An intense band also features in the 280–320 nm region and it is assigned to the inter-/intra-ligand π–π*/n–π* transition within the pyrazolyl-pyridazine bidentate ligand [26]. The absorption band (low intensity) in the region 450–470 nm is assigned to the Ru(II)-to-ligand charge transfer (MLCT). However, the intensities of the absorption bands for **Ru3** are weaker compared to those of **Ru1** or **Ru2**. In general, these observed spectral data are comparable to those of other [(η^6-arenes Ru(II) complexes bearing an N,N′ donor chelate [25]. As already stated, solutions of **Ru1-3** precipitate as orange crystalline solids. This shows that the halide ligand has little influence on the crystal field strength of the complexes. The presence of the 3-chloro-6-(1H-pyrazol-1-yl)pyridazine as a common spectator ligand and the LUMO fragment ensures an overriding metal-to-ligand charge transfer (MLCT) limited to a narrow range band gap (3.3–3.1 eV, see data in Table 3) between the three complexes. This leads to homologous halo-Ru(II) complexes with the same color.

Some of the vibrational stretching bands of **Ru1-3** (Figures S15–S17) shift to longer wavelengths compared to that of the free ligand, 3-chloro-6-(1H-pyrazol-1-yl)pyridazine (refer to Figure S14). This confirms the coordination of the bidentate ligand on the metal centers. As shown in Figures S15–S17, the FTIR spectra for **Ru1-3** feature common vibrational bands due to in-plane stretches of the C-C/N bonds of the *p*-cym and the pzn-pdzn bidentate ligands. This is an indication that the leaving halide group has minimum influence on the vibrational frequencies of the functional groups on the non-leaving ligands. The observed absorption bands are mainly due to the functional groups of the coordinated pzn-pdzn-N,N′ bidentate ligand, the *p*-cym ligands, and the borate counter ion. As an example, in Figure S15 (the spectrum of the **Ru1**), two absorption bands are observed at 3085 and 2873 cm^{-1}; these low-intensity bands are for the ν_{C-H} stretching frequencies for the aromatic and aliphatic stretches, respectively. Another common featuring band is the 1582 cm^{-1} (medium, $\nu_{C=N\ (pzn/pdzn)\ and}\ \nu_{N=N\ (pdzn)}$ stretch). The absorption bands of the cym occur as an intense duet at 1479 and 1404 cm^{-1} (intense, $\nu_{C=C(cym)}$ stretching). The bands that appear within the range 1200 and 1400 cm^{-1} (sharp, medium) are due to the $\nu_{C=C}$ vibration asymmetric stretches of the pzn/pdzn ring carbons. An intense absorption band is observed in the 1020–1051 cm^{-1} range due to the asymmetric stretching of the ν_{B-F} bond of the BF_4^- counter ion of **Ru1-3**. The sharp bands below 800 cm^{-1} (medium intensities) are due to the vibrational stretches of the Ru-C, Ru-$N_{pzn/pdzn}$, and Ru-Cl bonds. These frequency bands occur in the range reported in the literature [5,10,14,17,19].

2.3. DFT-Calculated Optimized Structures

Geometry-optimized structures for **Ru1-3** were computed in methanol as a solvent. The structures (see Table 4, first column) and the energies of the frontier molecular orbitals are presented in Table 4. Some of these DFT-calculated data were compared with the crystal structure (solid-state) and are presented in Tables 3 and 5.

Table 4. Overlays of the geometry-optimized structures on their crystal structures, and HOMO and LUMO electron density mappings for **Ru1-3**.

DFT-Optimized (Blue); Crystal Structure (Red)	**HOMO**	**LUMO**
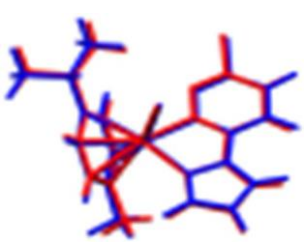 **Ru1**	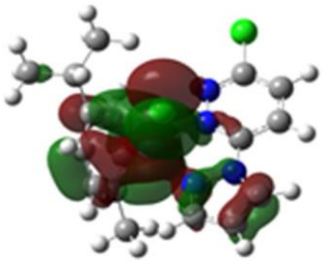	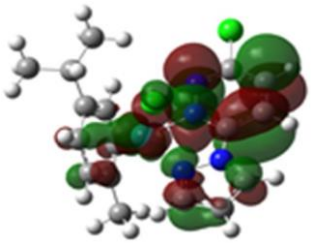
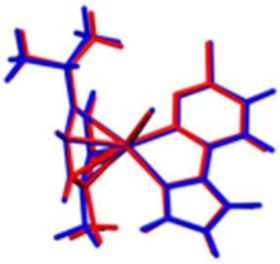 **Ru2**	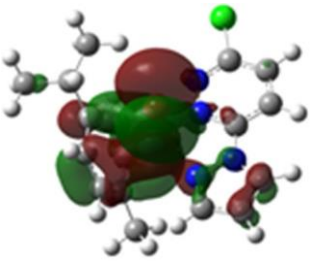	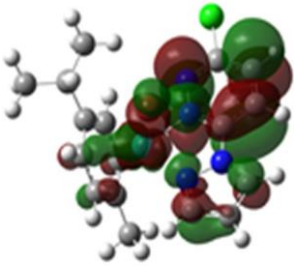
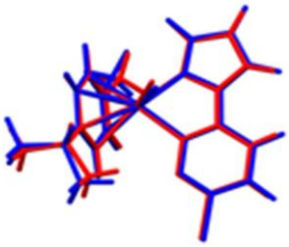 **Ru3**	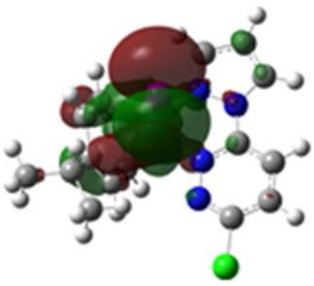	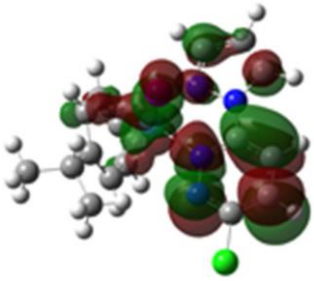

Table 5. Comparison of selected DFT data metrics with that from the crystal structure for complexes **Ru1-3**.

Bond Lengths	**Theoret.**	**Cryst.**	**%RE**	**Theoret.**	**Cryst**	**%RE**	**Theoret.**	**Cryst.**	**%RE**
Ru-‡X	2.3921	2.4529	2.5	2.5228	2.5982	2.9	2.6997	2.7644	6.5
$Ru\text{-}C_{Cym(centroid)}$	1.6760	1.8530	9.6	1.6760	1.8610	9.9	1.6790	1.8730	10.4
Ru-N1	2.0789	2.0458	1.6	2.0719	2.0452	1.3	2.0711	2.0439	1.3
Ru-N3	2.0802	2.0587	1.1	2.0743	2.0587	0.8	2.0731	2.0577	0.7

‡ X = Cl (**Ru1**); Br (**Ru2**); I (**Ru3**). Theoret. = DFT-calculated data; Cryst = crystal data taken as the accurate data; % % relative error (RE) = {(DFT Theoret. − Cryst)/Cryst} × 100.

The HOMO mappings of **Ru1-3** (Table 4) have a common distribution. They show significant electron density which is delocalized over the η⁶-cym ring, the Ru(II)-X (X = Cl, Br, I) bond, and the pzn donor arm. However, for **Ru3**, the density over the pzn is restricted only to the N donor atoms and is much smaller than that on the iodo ligand. For all, there is hardly any contribution to the HOMO by the pdzn ring for **Ru1-2**. This is as expected, since there is π- and σ-donation of electron density from their η⁶-cym and pzn rings, respectively. These donations reduce the effective positive charge on the Ru(II) ion, making it less electrophilic towards substituting nucleophiles. The LUMOs of **Ru1-3** are more localized on the pdzn rings. Conversely, there is no significant contribution to the LUMOs from the pzn rings. Thus, the electron density on the metal can easily be back-donated into π* orbitals of the pdzn ring than into the pzn donor arm. This means that the pdzn arm of the N,N′-bidentate is a π-acceptor comparable to pyridine or pyrazine. Overall, the N,N′ bidentate of these complexes can be an effective electron density modulator through a pull-and-push mechanism towards the Ru(II) metal center since pdzn is a better π-acceptor than pzn. This is important in producing complexes that have moderate reactivity and are therefore less prone to deactivation on transit to the cellular targets. Furthermore, the energy for **Ru3**′s LUMO is the highest, and hence this complex is the poorest π-acceptor, and least electrophilic. However, it is likely to be the most reactive towards incoming nucleophiles because its iodo ligand is the best leaving group due to the high polarizability of its metal bond.

To probe and predict the substitutional reactivity of **Ru1-3**, their HOMO-LUMO band gaps and global electrochemical descriptors (chemical hardness (η) [27], chemical potential (μ), electrophilicity (ω) [28], and charge density) were compared. As the halide, X is changed from Cl (**Ru1**) to I (**Ru3**), and the band gap, electronegativity, and η decrease; thus, **Ru1** is predicted to be the most stable and least reactive. The chemical potential, softness, and electrophilicity also increase from **Ru1** to **Ru3**, which is a clear indication of the greater ability of **Ru3** to accept electron density from the incoming nucleophile, thus enhancing the π-back bonding of electrons from the Ru into the π* orbital and stabilizing the transition state.

Looking at the calculated NBO charges in Table 4, the effective charge on the Ru(II) center decreases in the order **Ru1** > **Ru2** > **Ru3**. Thus, the charges on the complexes are affected by the nature of the leaving group. The Ru(II) ion in **Ru1** has the highest positive charge, indicating that it is the most electrophilic. **Ru3** is soft and has a high ability for accepting electrons from the soft Ru(II) ion, and hence is expected to be slightly more reactive than **Ru1** or **Ru2**. The large size of the atomic orbitals of the iodo ligand and hence its ease of polarizability results in an instantaneously large dipole that decreases the positive charge on the Ru(II). On one hand, the chloro ligand withdraws electron density from the metal center by resonance, which increases the positive charge on Ru(II). As a result, it is not the charge on the metal that determines reactivity, but rather the general increase in the negative charge on the ligand moiety, as indicated by electrophilicity indices [28].

Overlays of the DFT optimized structures (in methanol) of **Ru1-3** and their respective X-ray crystal structures show a good fit (root mean square deviation (*rmsd*) of < 2%) of the DFT-optimized structures. The superimposed structures are shown in the first column of Table 4. The computed length, distances, and angles are all within a 10% difference from the solid-state data (Tables S5–S10) from X-ray crystallographic analysis, thereby validating the accuracy of the theoretically calculated metric data of the complexes.

3. Materials and Methods

3.1. Reagents

The reagents and solvents used for the synthesis of the η⁶-*p*-cymene Ru(II) complexes were procured from commercial suppliers (Sigma Aldrich and Merck, Johannesburg, South Africa) and used without any further purification. The ligand 3-chloro-6-(1*H*-pyrazol-1-yl)pyridazine (pdzn-pzn) was prepared by following a literature procedure [29].

*3.2. Synthesis of [(η⁶-p-cymene)(3-chloro-6-(1H-pyrazol-1-yl)pyridazine)Ru(X)]BF₄, **Ru1** (X = Cl); **Ru2** (X = Br); **Ru3** (X = I)*

The complexes (**Ru1-3**) were all synthesized by the method of [20] with slight modifications in the purification stages. An acetonitrile solution (10 mL) of each of the precursor dimer complexes, [(η⁶-*p*-cymene)Ru(μ-X)(X)]₂, (X = Cl, Br, I), was prepared by dissolving 674, 869, and 1076 mg (1.1 mmol), respectively. The solution of each was separately added to 2.2 mmol (in acetonitrile) of 3-chloro-6-(1*H*-pyrazol-1-yl)pyridazine [29]. The respective mixture was stirred at room temperature for 4 h under an inert atmosphere of N_2 provided by the Schlenk line and accessories. This prevented the reactants from reacting with air. Thereafter, the mixture was concentrated under vacuo. About 5 mL of an ethanolic solution of NH_4BF_4 (2.5 mmol) was slowly added to precipitate the complexes. The mixtures were left under an ice bath for one hour, leading to the formation of orange crystalline precipitates. These were collected by filtration and washed with cold diethyl ether and dried under vacuo. The formation of the tetrafluoroborate salts is depicted in synthetic Scheme 1. Single crystals for X-ray diffraction analysis were grown by slow (1–2 weeks) diffusion of their vapors out of the methanol/diethyl ether solutions of **Ru1-Ru3**.

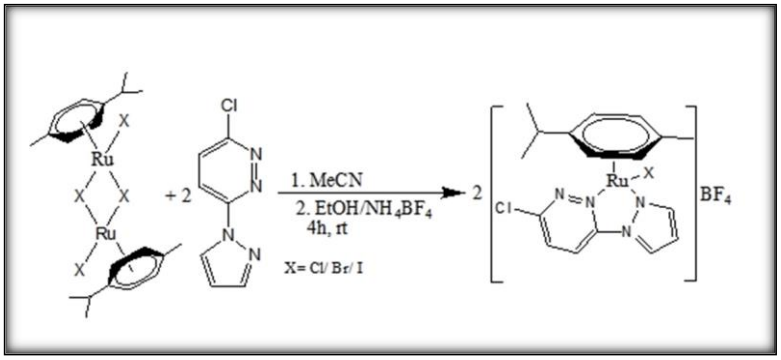

Scheme 1. Synthetic pathways for [(η⁶-*p*-cymene)(3-chloro-6-(1H-pyrazol-1-yl)pyridazine)Ru(X)]BF_4, **Ru1** (X = Cl); **Ru2** (X = Br); **Ru3** (X = I) complexes.

3.3. Characterization of Complexes

^1H and ^{13}C NMR spectra were recorded on a Bruker Avance DPX 500 MHZ spectrometer (Bruker BioSpin GmbH, Rheinstetten, Germany) fitted with a 5 mm sample probe at 30 °C to confirm the purity and identity of the compounds. All chemical shifts of protons or carbons of 3-chloro-6-(1*H*-pyrazol-1-yl)pyridazine are reported relative to those of tetramethyl silane ($SiMe_4$). The mass spectral data of the ligands and complexes were acquired on an LC Premier micro-mass spectrometer. FTIR spectra of complexes were recorded (in KBr) on the Agilent Technologies Cary 630 spectrometer (Vienna, Austria) in the 3800–600 cm^{-1} range. The UV–visible absorption spectra were acquired on a carry 100 Bio UV-visible spectrophotometer with a temperature controller of ± 0.05 °C. Elemental compositions (CHN) of **Ru1-3** were determined on a Thermo Scientific Flash 2000 Spectrometer. The characterization data are given in the Supporting Information (SI). Single-crystal X-ray crystallographic data of **Ru1-3** were collected on a Bruker APEX Duo CCD area detector diffractometer [30] with an Incoatec microsource operating at 30 W of power. The crystal was kept at a constant temperature within the range of 99.9–104 K during data collection using an Oxford Instruments Cryojet accessory (Oxford, UK). Diffraction was by graphite-monochromated Cu K_α radiation (λ = 1.54178 Å) at a crystal-to-detector distance of 50 mm. Data collection was conducted at the following set conditions: ω-/φ-scans with exposures, taken at 30 W X-ray power and 0.50 frame widths, 2θ range in the range 6.98–142.948° using SAINTS´ APEX2 [31]. The crystal structures were solved by the OLEX2 program [32], using the SHELXT [33] structure solution programs and Intrinsic Phasing and refined by SHELXL [31] refinement programs. The non-hydrogen atoms were refined anisotropically by full-matrix least-squares minimization/refinement of F^2. Hydrogen atoms were

included but not refined. Visualization of the crystallographic data was performed in Mercury v.4.3 (Cambridge Crystallographic Data Centre, Cambridge, UK), and the crystal data are given in Tables S2–S10.

*3.4. DFT-Optimized Structures of **Ru1-3***

The Density Functional Theory (DFT) ground state-optimized structures of **Ru1-3** were calculated using the Gaussian 09 program suite [34]. The B3LYP method [35,36], utilizing the LANL2DZ basis sets, was used to optimize the geometry of the complexes. Calculations were simulated in methanol using the conductor-like polarizable continuum model (C-PCM) [37,38].

*3.5. Listed Spectral Data of **Ru1-3***

3-chloro-6-(1H-pyrazol-1-yl)pyridazine (**N,N^{I}-*L***): White powder, ^{1}H NMR (500 MHz, d_6-DMSO) δ (ppm), 8.80 (d, J = 2.5 Hz, 1H$_{pzn}$), 8.27 (d, J = 9.3 Hz, 1H$_{pzn}$), 8.08 (d, J = 9.1 Hz, 1H$_{pdzn}$), 7.98 (d, J = 1.4 Hz, 1H$_{pdzn}$), 6.70 (dd, J = 4.3 Hz, 1H$_{pzn}$). ^{13}C (100 MHz, d_6-DMSO): δ (ppm) 154.1 (N-C-N$_{pdzn}$), 153.7 (N=C-Cl, $_{pdzn}$), 143.7 (C=N, $_{pzn}$), 131.8 (C=C$_{pdzn}$), 127.8, (C=N$_{pzn}$), 120.9 (C=C$_{pdzn}$), 109.7 (C=C$_{pzn}$) (see also Figure S14).

[(η^6-p-cymene)(3-chloro-6-(1H-pyrazol-1-yl)pyridazine)Ru(Cl)]BF$_4$ (**Ru1**): Yield 74.2%, orange crystals, MS (ESI)$^+$ *m/z* (% I_{pic}) = 451 (100), [C$_{17}$H$_{19}$ClN$_4$RuCl + H]$^+$; ^{1}H NMR (500 MHz, d_6-DMSO) δ (ppm), 9.18 (d, J = 3.2 Hz, 1H$_{pzn}$), 9.02 (d, J = 2.2 Hz, 1H$_{pzn}$), 8.80 (d, J = 9.3 Hz, 1H$_{pdzn}$), 8.58 (d, J = 9.3 Hz, 1H$_{pdzn}$) 7.17 (dd, J = 3.2, 2.2 Hz, 1H$_{pzn}$), 6.17 (ddd, J = 12.1, 6.2, 1.1 Hz, 2H$_{Ar\ p\text{-}Cym}$), 5.99 (dd, J = 6.1, 1.1 Hz, 1H,$_{Ar\ p\text{-}Cym}$), 5.87 (dd, J = 6.2, 1.1 Hz, 1H$_{p\text{-}Cym}$), 2.79 (p, J = 13.8, 6.9 Hz, 1H$_{p\text{-}Cym}$, CH$_{(isopropyl)}$, 2.12 (s, 3H$_{p\text{-}Cym}$, CH$_3$), 1.15 (t, J = 6.9 Hz 6H$_{p\text{-}Cym}$, CH$_{3(isopropyl)}$. ^{13}C (100 MHz, d_6-DMSO): δ (ppm) 153.7 (N-C-N$_{pdzn}$), 150.9 (C=N$_{pzn}$), 148.8 (N=C-Cl$_{pdzn}$), 134 (C=C$_{pdzn}$), 132.9 (C=N$_{pzn}$), 121.9 (C=C$_{pdzn}$), 112.8 (C=C$_{pzn}$), 105, 101.9, 86.7, 86.6, 84.2, 84.1 (C$_{Ar\ p\text{-}Cym}$), 30.3 C$_{p\text{-}Cym}$, CH$_{isopropyl}$, 21.9 (-CH$_{3p\text{-}Cym}$), 21.3, 17.8 (-CH$_{3\ isopropyl\ p\text{-}Cym}$). FTIR (KBr, cm^{-1} $_{[(weak/medium/strong/sharp/broad\ =\ w/m/s/(shrp/br))]}$: 3085$_{w(}$ν $_{(Carom\text{-}H)}$; 2959$_{w,}$ ν $_{(C\text{-}Haliphatic),}$ w$_{(br)}$; 1582, w(shrp), ν(N=C$_{pdzn/pzn}$); 1480, 1404, s$_{shrp}$, ν(C=C$_{cym/pzn/,pdzn}$); 1284, m$_{(shrp)}$, ν(Ar βCHcym); 1050.37, vs$_{(shrp)}$, ν(BF$_4^-$); 820–850, 780, 650, m$_{shrp}$ ν[(Ru-N$_{pdzn/pzn}$, Ru-C$_{centroid\ cym}$, Ru-Cl], respectively. Elemental analysis: Calculated for [C$_{17}$H$_{19}$ClN$_4$RuCl]BF$_4$, %: C 37.94; H, 3.56; N, 10.41; found, % C, 37.82; H, 3.56; N, 10.50.

[(η^6-p-cymene)(3-chloro-6-(1H-pyrazol-1-yl)pyridazine)Ru(Br)]BF$_4$ (**Ru2**): Yield 75.5%, orange crystals, MS (ESI)$^+$ *m/z* (% I_{pic}) = 497 (100), [C$_{17}$H$_{19}$ClN$_4$RuBr + H]$^+$; ^{1}H NMR (500 MHz, d_6-DMSO) δ (ppm), 9.18 (d, J = 3.2 Hz, 1H$_{pzn}$), 8.99 (d, J = 2.1 Hz, 1H$_{pzn}$), 8.78 (d, J = 9.3 Hz, 1H$_{pdzn}$, 8.57 (d, J = 9.3 Hz, 1H$_{pdzn}$), 7.17 (dd, J = 3.2, 2.1 Hz, 1H$_{pzn}$), 6.16 (m, 2H$_{Ar\text{-}p\text{-}Cym}$), 5.99 (m, 1H$_{p\text{-}Cym}$), 5.88 (dd, J = 6.3, 1.2 Hz, 1H$_{p\text{-}Cym}$), 2.86 (h, J = 6.9 Hz, 1H CH$_{isopropyl\ p\text{-}Cym}$, 2.17 (s, 3H, $_{p\text{-}Cym}$, CH$_3$), 1.17 (dd, J = 8.6, 6.9 Hz, 6H, -CH$_{3isopropyl\ p\text{-}Cym}$). ^{13}C (100 MHz, d_6-DMSO): δ (ppm) 153.6 (N-C-N$_{pdzn}$), 150.8 (C=N, $_{pzn}$), 149.1 (N=C-Cl, $_{pdzn}$), 133.9 (C=C$_{pdzn}$), 132.9, (C=N$_{pzn}$), 121.8 (C=C$_{pdzn}$), 112.9 (C=C$_{pzn}$), 105.4, 101.8, 86.6, 84.6, 84.5$_{Ar,\ p\text{-}cym}$, 30.3 CH$_{isopropyl)}$, 21.9 (-CH$_{3p\text{-}Cym}$), 21.3, 17.8, (-CH$_{3isopropyl\ p\text{-}Cym}$). FTIR (KBr, cm^{-1}, w/m/s$_{shrp/br}$ (= weak/medium/strong$_{sharp/broad}$): 3083, w, ν(C$_{arom}$-H); 2875-3, w, ν(C-H$_{aliphatic}$), w$_{(br)}$; 1582, w(shrp), ν(N=C$_{pdzn/pzn}$); 1480, 1403, s$_{shrp}$, ν(C=C$_{cym/pzn/,pdzn}$); 1168, m$_{(shrp)}$, ν(Ar βCHcym); 1021, vs$_{(shrp)}$, ν(BF$_4$); 820–50, 780, 650, m$_{shrp}$ ν[(Ru-N$_{pdzn/pzn}$, Ru-C$_{centroid\ cym}$, Ru-Cl], respectively. Elemental analysis: Calculated for [C$_{17}$H$_{19}$ClN$_4$RuBr]BF$_4$, %: C 35.05; %H, 3.29; N, 9.62; found, % C, 35.72; H, 3.08; N, 9.48.

[(η^6-p-cymene)(3-chloro-6-(1H-pyrazol-1-yl)pyridazine)Ru(I)]BF$_4$ (**Ru3**): Yield 40%, orange crystals. MS (ESI)$^+$ *m/z* (% I_{pic}) = 543 (100), [C$_{17}$H$_{19}$ClN$_4$RuI + H]$^+$; ^{1}H NMR (500 MHz, d_6-DMSO) δ (ppm), 9.19 (d, J = 3.2 Hz, 1H$_{pzn}$), 8.94 (d, J = 2.2 Hz, 1H$_{pzn}$), 8.78 (d, J = 9.3 Hz, 1H$_{pdzn}$, 8.55 (d, J = 9.3 Hz, 1H$_{pdzn}$), 7.17 (dd, J = 3.2, 2.2 Hz, 1H$_{pzn}$), 6.21 (dd, 1H, J = 6.4, 1.3 Hz), 6.14 (dd, J = 6.2, 1.2 Hz, 1H$_{p\text{-}Cym}$, 5.99 (dd, J = 6.4, 1.3 Hz, 1H$_{Ar\text{-}p\text{-}Cym}$), 5.94 (dd, J = 6.2, 1.2 Hz, 1H$_{p\text{-}Cym}$, 2.97 (h, J = 6.9 Hz, 1H, $_{p\text{-}Cym}$, CH$_{isopropyl}$, 2.21 (s, 3H,

$CH_{3\ p\text{-Cym}}$), 1.19 (d, J = 11.0, 6.9 Hz, 6H, $CH_{3isopropyl,\ p\text{-Cym}}$). ^{13}C (100 MHz, d_6-DMSO): δ (ppm) 153.5 (N-C-N_{pdzn}), 150.3 (C=N_{pzn}, 149.8 (N=C-Cl_{pdzn}), 133.7 (C=C_{pdzn}), 133 (C=N_{pzn}), 121.5 (C=C_{pdzn}), 113.5 (C=C_{pzn}), 106.0, 102.2, 86.8, 86.5, 85.5, 84.9 ($Ar_{p\text{-Cym}}$), 31.1 ($CH_{,isopropyl\ p\text{-Cym}}$, 22.8 (-$CH_{3p\text{-Cym}}$, 19.1, 21.9, -$CH_{3isopropyl\ p\text{-Cym}}$). FTIR (KBr, cm^{-1}, w/m/$s_{shrp/br}$ (= weak/medium/$strong_{sharp/broad}$), $\nu_{(funct.\ gr)}$): 3107, w, ν(C_{arom}-H); 2976, w, ν(C-$H_{aliphatic}$), $w_{(br)}$; 1581, w(shrp), ν(N=$C_{pdzn/pzn}$); 1433, s_{shrp}, ν(C=$C_{cym/pzn/,pdzn}$); 1284, $m_{(shrp)}$, ν(Ar βCHcym); 1030, $vs_{(shrp)}$, ν(BF_4); 820–50, 780, 650, m_{shrp} ν[(Ru-$N_{pdzn/pzn}$, Ru-$C_{centroid.\ cym}$, Ru-Cl], respectively]. Elemental analysis: Calculated for [$C_{17}H_{19}ClN_4RuI$]BF_4, %: C 32.43; %H, 3.04; N, 8.90; found, % C, 32.92; H, 3.32; N, 9.07. 4.

4. Conclusions

Three borate salts of half-sandwich Ru(II) complexes, [(η6-*p*-cymene)(3-chloro-6-(1*H*-pyrazol-1-yl)pyridazine)Ru(X)]BF_4 (X = Cl (Ru1), Br (**Ru2**), or I (**Ru3**)), were synthesized from the reactions of their respective dimer precursors, [(η^6-*p*-cymene)Ru(μ-X)(X)]$_2$ (X = Cl, Br, I), with two-mole equivalents of 3-chloro-6-(1*H*-pyrazol-1-yl)pyridazine under inert conditions and subsequent precipitation by the addition of excess BF_4^- ions. Orange crystalline precipitates were obtained in good yields, from which respective single crystals for X-ray diffraction analysis were crystallized by slow evaporation from their methanolic/diethyl ether solutions. Complete characterization of all complexes was achieved using ^1H and ^{13}C NMR, FTIR and UV-visible absorption spectroscopies, elemental analysis, and single-crystal X-ray crystallography. The η^6-cym group is facially coordinated to the Ru(II) ion and occupies the apex position of the pseudo-octahedral geometry. The pyrazole and pyridazine donor arms of the ancillary N,N′-bidentate (3-chloro-6-(1*H*-pyrazol-1-yl)pyridazine) and a halide occupy the other sites of the piano stool geometry. DFT computed data show that the nature of the leaving group affects the effective charge electrophilicity, and hence the reactivity of the complex. **Ru3** has the greatest tendency to accept the electron density of incoming nucleophiles during a ligand substitution process.

Supplementary Materials: You can access the following information online. Spectral characterization data: Figures S1–S17, including the COSY and HSQC 2D-NMR spectral data. Tables of data: Table S1, 2D-NMR data; Tables S2–S4, the atomic coordinates for **Ru1-3**, and Tables S5–S10, comparable isotropic displacement parameters (2×10^3), bond lengths (Å), and angles [°] for **Ru1-3**; Table S11, the short-contacts/non-conventional hydrogen contacts.

Author Contributions: A.K.K.: Investigation, conceptualization, synthesis, drafting; P.O.: conceptualization, partial resourcing supervision; J.G.: partial resourcing on synthesis, reviewing; R.O.O.: crystallization, spectral characterization and reviewing, L.A.H.: DFT computations, X-ray diffraction data collection, visualization, handling, and analysis; A.M.: DFT and X-ray diffraction data analyses and partial resourcing on the characterization of compounds, and drafting and reviewing. All authors have read and agreed to the published version of the manuscript.

Funding: This research received no external funding.

Data Availability Statement: The supplementary crystallographic data for **Ru1-3** (ref code: cu_am_ro_am_3a-c_0m; CDCC numbers: 2194343, 2194345, and 2194346, respectively) can be obtained free of charge via http://www.ccdc.cam.ac.uk/conts/retrieving.html (accessed on 3 August 2022), or from the Cambridge Crystallographic Data Centre, 12 Union Road, Cambridge CB2 1EZ, U.K.; fax: (+44)1223-336-033; or via email: deposit@ccdc.cam.ac.uk.

Acknowledgments: We acknowledge the Department of Chemistry at Egerton University in Kenya, where the conception and synthesis of the complexes were carried out. This work's partial financing is credited to the Research Office of the University of KwaZulu-Natal (UKZN), RSA. The DFT, crystallization, and single-crystal X-ray diffraction analysis were carried out at the UKZN's School of Chemistry and Physics, PMB Campus. We thank C.J.Van Rensburg for assistance in mass spectroscopic analysis and C.Grimmer for NMR analysis.

Conflicts of Interest: No potential conflict of interest or competing interest are foreseen.

References

1. Gichumbi, J.M.; Friedrich, H.B. Half-sandwich complexes of platinum group metals (Ir, Rh, Ru and Os) and some recent biological and catalytic applications. *J. Organomet. Chem.* **2018**, *866*, 123–143. [CrossRef]
2. Canivet, J.; Karmazin-Brelot, L.; Süss-Fink, G. Cationic arene ruthenium complexes containing chelating 1, 10-phenanthroline ligands. *J. Organomet. Chem.* **2005**, *690*, 3202–3211. [CrossRef]
3. Mendoza-Ferri, M.G.; Hartinger, C.G.; Eichinger, R.E.; Stolyarova, N.; Severin, K.; Jakupec, M.A.; Nazarov, A.A.; Keppler, B.K. Influence of the spacer length on the in vitro anticancer activity of dinuclear Ruthenium—Arene compounds. *Organometallics* **2008**, *27*, 2405–2407. [CrossRef]
4. Mendoza-Ferri, M.G.; Hartinger, C.G.; Nazarov, A.A.; Eichinger, R.E.; Jakupec, M.A.; Severin, K.; Keppler, B.K. Influence of the arene ligand, the number and type of metal centers, and the leaving group on the in vitro antitumor activity of polynuclear organometallic compounds. *Organometallics* **2009**, *28*, 6260–6265. [CrossRef]
5. Matveevskaya, V.V.; Pavlov, D.I.; Samsonenko, D.G.; Ermakova, E.A.; Klyushova, L.S.; Baykov, S.V.; Boyarskiy, V.P.; Potapov, A.S. Synthesis and structural characterization of half-sandwich arene–ruthenium(II) Complexes with *bis*(imidazol-1-yl)methane, Imidazole and Benzimidazole. *Inorganics* **2021**, *9*, 34. [CrossRef]
6. Gichumbi, J.M.; Friedrich, H.B.; Omondi, B.; Lazarus, G.G.; Singh, M.; Chenia, H.Y. Synthesis, characterization, anticancer and antimicrobial study of arene ruthenium(II) complexes with 1,2,4-triazole ligands containing an α-diimine moiety. *Z. Naturforsch. B* **2018**, *73*, 167–178. [CrossRef]
7. Rademaker-Lakhai, J.M.; Van Den Bongard, D.; Pluim, D.; Beijnen, J.H.; Schellens, J.H. A phase I and pharmacological study with imidazolium-*trans*-DMSO-imidazole-tetrachlororuthenate, a novel ruthenium anticancer agent. *Clin. Cancer Res.* **2004**, *10*, 3717–3727. [CrossRef]
8. Brindell, M.; Stawoska, I.; Supel, J.; Skoczowski, A.; Stochel, G.; van Eldik, R. The reduction of (ImH)[trans-Ru(III)Cl_4(dmso)(Im)] under physiological conditions: Preferential reaction of the reduced complex with human serum albumin. *JBIC* **2008**, *13*, 909–918. [CrossRef]
9. Mahmud, K.M.; Niloy, M.S.; Shakil, M.S.; Islam, M.A. Ruthenium Complexes: An alternative to platinum drugs in colorectal cancer treatment. *Pharmaceutics* **2021**, *13*, 1295. [CrossRef]
10. Monro, S.; Colon, K.L.; Yin, H.; Roque III, J.; Konda, P.; Gujar, S.; Thummel, R.P.; Lilge, L.; Cameron, C.G.; McFarland, S.A. Transition metal complexes and photodynamic therapy from a tumor-centered approach: Challenges, opportunities, and highlights from the development of TLD1433. *Chem. Rev.* **2018**, *119*, 797–828. [CrossRef]
11. Gichumbi, J.M.; Omondi, B.; Lazarus, G.; Singh, M.; Shaikh, N.; Chenia, H.Y.; Friedrich, H.B. Influence of halogen substitution in the ligand sphere on the antitumor and antibacterial activity of half-sandwich ruthenium(II) complexes [RuX(η^6-arene)($C_5H_4N_2$-CH=N-Ar)]$^+$. *ZAAC* **2017**, *643*, 699–711. [CrossRef]
12. Zeng, L.; Gupta, P.; Chen, Y.; Wang, E.; Ji, L.; Chao, H.; Chen, Z.S. The development of anticancer ruthenium(II) complexes: From single molecule compounds to nanomaterials. *Chem. Soc. Rev.* **2017**, *46*, 5771–5804. [CrossRef] [PubMed]
13. Mitra, R.; Samuelson, A.G. Substitution-modulated anticancer activity of half-sandwich ruthenium(II) complexes with heterocyclic ancillary ligands. *Eur. J. Inorg. Chem* **2014**, *2014*, 3536–3546. [CrossRef]
14. Romero-Canelón, I.; Salassa, L.; Sadler, P.J. The contrasting activity of iodido versus chlorido ruthenium and osmium arene azo-and imino-pyridine anticancer complexes: Control of cell selectivity, cross-resistance, p53 dependence, and apoptosis pathway. *J. Med. Chem.* **2013**, *56*, 1291–1300. [CrossRef]
15. Gumus, S. A computational study on substituted diazabenzenes. *Turk. J. Chem.* **2011**, *35*, 803–808. [CrossRef]
16. Imran, M.; Asif, M. Study of various pyridazine and phthalazine drugs with diverse therapeutical and agrochemical activities. *Russ. J. Bioorg. Chem.* **2020**, *46*, 745–767. [CrossRef]
17. Morris, R.E.; Aird, R.E.; del Socorro Murdoch, P.; Chen, H.; Cummings, J.; Hughes, N.D.; Parsons, S.; Parkin, A.; Boyd, G.; Jodrell, D.I. Inhibition of cancer cell growth by ruthenium(II) arene complexes. *J. Med. Chem.* **2001**, *44*, 3616–3621. [CrossRef]
18. Gupta, G.; Prasad, K.T.; Das, B.; Yap, G.P.; Rao, K.M. Ruthenium half-sandwich complexes with tautomerized pyrazolyl-pyridazine ligands: Synthesis, spectroscopic and molecular structural studies. *J. Organomet. Chem.* **2009**, *694*, 2618–2627. [CrossRef]
19. Albertin, G.; Antoniutti, S.; Castro, J.; Garcí-Fontán, S. Preparation of pyrazole-pyrazolate half-sandwich complexes of ruthenium and osmium. *Eur. J. Inorg. Chem* **2011**, *2011*, 510–520. [CrossRef]
20. Gichumbi, J.M.; Friedrich, H.B.; Omondi, B. Synthesis and characterization of half-sandwich ruthenium(II) complexes with N-alkylpyridyl-imine ligands and their application in transfer hydrogenation of ketones. *Transit. Metal Chem.* **2016**, *41*, 867–877. [CrossRef]
21. Gichumbi, J.M.; Friedrich, H.B.; Omondi, B. Crystal structure of chlorido-(η^6–1-isopropyl-4-methyl benzene)-(1-(pyridin-2-yl)-N-(p-tolyl)methanimine-κ^{2}N,N)ruthenium(II) hexafluorophosphate(V), $C_{23}H_{26}ClF_6N_2PRu$. *Z. Krist. New Cryst. Struct.* **2017**, *232*, 285–287. [CrossRef]
22. Neels, A.; Stoeckli-Evans, H.; Plasseraud, L.; Fidalgo, E.G.; Süss-Fink, G. Di-μ-bromo-bis [bromo(η^6-para-cymene)ruthenium(II)] benzene solvate and di-μ-iodo-bis [(η^6-para-cymene)iodoruthenium(II)] toluene solvate. *Acta Crystallogr. Sect. C Cryst. Struct. Commun.* **1999**, *55*, 2030–2032. [CrossRef]
23. Bacchi, A.; Cantoni, G.; Pelagatti, P. Polymorphs and co-crystal with half-sandwich Ru(II) dimers [(η^6-arene) $RuX_2]_2$. *CrystEngComm* **2013**, *15*, 6722–6728. [CrossRef]

24. Wang, H.Y.; Qian, Y.; Wang, F.X.; Habtemariam, A.; Mao, Z.W.; Sadler, P.J.; Liu, H.K. Ruthenium(II)–Arene Metallacycles: Crystal Structures, Interaction with DNA, and Cytotoxicity. *Eur. J. Inorg. Chem* **2017**, *2017*, 1792–1799. [CrossRef]
25. Gupta, G.; Prasad, K.T.; Rao, A.V.; Geib, S.J.; Das, B.; Rao, K.M. Novel mononuclear η^5-pentamethylcyclopentadienyl complexes of platinum group metals bearing pyrazolylpyridazine ligands: Syntheses and spectral studies. *Inorg. Chim. Acta* **2010**, *363*, 2287–2295. [CrossRef]
26. Gichumbi, J.M.; Friedrich, H.B.; Omondi, B. Solvato-polymorph of $[(\eta^6\text{-}C_6H_6)RuCl\ (L)]PF_6$ (L=(2, 6-dimethyl-phenyl-pyridin-2-ylmethyleneamine). *J. Mol. Struct.* **2016**, *1113*, 55–59. [CrossRef]
27. Desoize, B.; Madoulet, C. Particular aspects of platinum compounds used at present in cancer treatment. *Crit. Rev. Oncol. Hematol.* **2002**, *42*, 317–325. [CrossRef]
28. Wekesa, I.M.; Jaganyi, D. Kinetic and mechanistic studies of 1, 3-bis(2-pyridylimino)isoindolatePt(II) derivatives. Experimental and new computational approach. *Dalton Trans.* **2014**, *43*, 2549–2558. [CrossRef]
29. Thompson, L.K.; Woon, T.; Murphy, D.B.; Gabe, E.J.; Lee, F.L.; Le Page, Y. Binuclear copper(II) complexes of a series of tetradentate pyrazolyldiazines. Crystal and molecular structures of [μ-3,6-bis (3,5-dimethyl-1-pyrazolyl)pyridazine-N,μ-N^3,μ-N^3,N](μ-hydroxo)dichlorodicopper(II)aquotrichlorocuprate hydrate, $Cu_3C_{14}H_{21}Cl_5N_6O_3$, and [μ-3,6-bis (3, 5-dimethyl-1-pyrazolyl)pyridazine-N,μ-N^6,μ-N^7, N](μ-hydroxo)tris(nitrato)diaquodicopper(II) hydrate, $Cu_2C_{14}H_{23}N_9O_{13}$. *Inorg. Chem.* **1985**, *24*, 4719–4725. [CrossRef]
30. CCD CrysAlis. *CrysAlis Red*; Xcalibur PX Software; Oxford Diffraction Ltd.: Abingdon, UK, 2008.
31. Bruker APEX2. *SAINT and SADABS*; Bruker AXS Inc.: Madison, WI, USA, 2009.
32. Dolomanov, O.; Bourhis, L.; Gildea, R.; Howard, J.; Puschmann, H. OLEX2: A complete structure solution, refinement and analysis program. *J. Appl. Cryst.* **2009**, *42*, 339–341. [CrossRef]
33. Sheldrick, G.M. SHELXT–Integrated space-group and crystal-structure determination. *Acta Crystallogr. A Found. Adv.* **2015**, *71*, 3–8. [CrossRef] [PubMed]
34. Frisch, M.; Trucks, G.W.; Schlegel, H.B.; Scuseria, G.E.; Robb, M.A.; Cheeseman, J.R.; Scalmani, G.; Barone, V.; Mennucci, B.; Petersson, G. *Gaussian 09, Revision D. 01*; Gaussian, Inc.: Wallingford, CT, USA, 2009.
35. Lee, C.; Yang, W.; Parr, R.G. Development of the Colle-Salvetti correlation-energy formula into a functional of the electron density. *Phys. Rev. B* **1988**, *37*, 785–789. [CrossRef] [PubMed]
36. Becke, A.D. Becke's three parameter hybrid method using the LYP correlation functional. *J. Chem. Phys.* **1993**, *98*, 5648–5652. [CrossRef]
37. Barone, V.; Cossi, M. Quantum calculation of molecular energies and energy gradients in solution by a conductor solvent model. *J. Phys. Chem. A* **1998**, *102*, 1995–2001. [CrossRef]
38. Cossi, M.; Rega, N.; Scalmani, G.; Barone, V. Energies, structures, and electronic properties of molecules in solution with the C-PCM solvation model. *J. Comput. Chem.* **2003**, *24*, 669–681. [CrossRef]